The Journal of Neuroscience

Nonlinear interaction between shunting and adaptation controls a switch between integration and coincidence detection in pyramidal neurons

Journal:	*Journal of Neuroscience*
Manuscript ID:	draft
Manuscript Type:	Regular Manuscript
Manuscript Section:	Cellular/Molecular - Laurence Trussell
Date Submitted by the Author:	n/a
Complete List of Authors:	Prescott, Steven; Salk Institute, Computational Neurobiology Laboratory Ratté, Stéphanie; Université de Montréal, Département de physiologie De Koninck, Yves; Centre de Recherche Université Laval Robert-Giffard, Division de Neurobiologie Cellulaire; McGill University, Department of Pharmacology and Therapeutics Sejnowski, Terrence; Salk Institute, Howard Hughes Medical Institute; University of California, San Diego, Division of Biological Sciences
Keywords:	AHP current, coincidence detector, integrator, M current, membrane conductance, spike-time precision
Themes & Topics:	Modulation of neuronal firing properties < Intrinsic Membrane Properties < Theme B: Neural Excitability, Synapses and Glia: Cellular Mechanisms

Section: Cellular/Molecular Neuroscience

Senior editor: Laurence O. Trussell

Nonlinear interaction between shunting and adaptation controls a switch between integration and coincidence detection in pyramidal neurons

Abbreviated title: Interaction between shunting and adaptation

Steven A. Prescott[1], Stéphanie Ratté[2], Yves De Koninck[3], and Terrence J. Sejnowski[1,4]

[1]Computational Neurobiology Laboratory, Howard Hughes Medical Institute, Salk Institute, La Jolla, CA 92037
[2]Département de physiologie, Université de Montréal, Montréal, Québec, Canada H3C 3J7
[3]Division de Neurobiologie Cellulaire, Centre de Recherche Université Laval Robert-Giffard, Québec, Québec, Canada G1J 2G3, and Department of Pharmacology and Therapeutics, McGill University, Montréal, Québec, Canada H3A 1Y6
[4]Division of Biological Sciences, University of California, San Diego, La Jolla, CA 92093

Corresponding Author:
Steven A. Prescott
Computational Neurobiology Laboratory, Salk Institute
10010 North Torrey Pines Rd., La Jolla, CA 92037
Phone: 858-453-4100 x1215
Fax: 858-587-0417
E-mail: sprescott@salk.edu

Number of text pages: 35

Number of figures: 8

Keywords: AHP current, coincidence detector, integrator, M current, membrane conductance, spike-time precision.

Acknowledgements: We wish to thank Bard Ermentrout for assistance using XPPAUT. This research was supported by the Natural Sciences and Engineering Research Council of Canada (YDK) and by the Howard Hughes Medical Institute (TJS). SAP was supported by a postdoctoral fellowship from the Canadian Institutes of Health Research.

ABSTRACT

The membrane conductance of a pyramidal neuron *in vivo* is substantially increased by background synaptic input. Increased membrane conductance, or shunting, does not simply reduce neuronal excitability. Recordings from hippocampal pyramidal neurons revealed that adaptation caused complete cessation of spiking in the high conductance state, whereas repetitive spiking could persist despite adaptation in the low conductance state. This behavior was reproduced in a phase plane model and was explained by an increase in voltage threshold caused by shunting. Increase in threshold allows greater adaptation to be induced at subthreshold potentials and reduces the minimum adaptation required to stabilize the system. Because this phenomenon depends on adaptation's activation curve, it occurs with M current-mediated adaptation but not with AHP current-mediated adaptation. The nonlinear interaction between shunting and the M current has other important consequences. First, timing of spikes elicited by brief stimuli is more precise when background spikes elicited by sustained input are prohibited, as occurs exclusively with M current-mediated adaptation in the high conductance state. Second, activation of the M current at subthreshold potentials, which is increased in the high conductance state, hyperpolarizes average membrane potential away from voltage threshold, allowing only large, rapid fluctuations to reach threshold and elicit spikes. These results suggest that the shift from a low to high conductance state in a pyramidal neuron is accompanied by a switch from encoding DC input with firing rate to encoding transient inputs with precisely timed spikes, in effect, switching the operational mode from integration to coincidence detection.

Under *in vivo* conditions, the background synaptic activity experienced by pyramidal neurons can dramatically increase total membrane conductance. Input resistance (R_{in}) may drop by as much as 80%, and is accompanied by shortening of both the membrane time constant and length constant (Bernander et al., 1991; Paré et al., 1998; Destexhe and Paré, 1999). These changes have profound effects on the spatiotemporal integration of synaptic inputs (Destexhe et al., 2003; Shu et al., 2003; Rudolph and Destexhe, 2003). An increase in membrane conductance, or shunting, can also influence the capacity of neurons to spike repetitively during sustained stimulation; for example, damage caused by impalement with a sharp electrode can introduce a leak conductance (Staley et al., 1992) that results in the neuron firing few if any spikes during prolonged current injection, whereas the same neuron may fire repetitively if not damaged (Alger et al., 1984).

Spike frequency adaptation is another process that modulates repetitive spiking, and refers to the reduction of firing rate during sustained stimulation. Strength of adaptation varies among pyramidal neurons (Barkai and Hasselmo, 1994) and can itself be modulated (Nicoll, 1988). Within pyramidal neurons, adaptation can be mediated by slow, voltage-sensitive potassium currents (e.g. M current), by calcium-sensitive potassium currents (e.g. AHP current), or by a combination of both (Madison and Nicoll, 1984; Storm, 1990; Sah and Davies, 2000; Gu et al., 2005). Although the M and AHP currents are quite distinct in terms of their basis for activation, the effects of those two currents are often considered equivalent insofar as they both reduce firing rate once activated. Data presented here challenge that view, showing that the difference in activation requirements has important consequences for the outcome of adaptation, specifically whether adaptation prevents repetitive spiking or simply reduces its rate, which in turn has implications for other response properties like spike-time precision.

If both shunting and adaptation modulate repetitive firing, the question arises as to how those two mechanisms interact. Experimental data from CA1 pyramidal neurons revealed that they do indeed interact, and that they do so in a nonlinear manner. In order to investigate that interaction we developed a simplified phase plane model that reproduced the experimental data.

Phase plane analysis facilitates the visualization of complex dynamical problems and, in that regard, has been particularly useful for investigating neuronal excitability (FitzHugh, 1961; FitzHugh, 1969; Rinzel, 1985; Rinzel and Ermentrout, 1998; Izhikevich, 2000). This approach was used here to demonstrate how changes in membrane conductance influence the induction and outcome of adaptation, depending on the activation properties of the underlying current. Further investigation revealed this nonlinear interaction between shunting and adaptation to have important consequences for whether a pyramidal neuron encodes inputs as an integrator or as a coincidence detector.

MATERIALS AND METHODS

Electrophysiology

All experiments were done in accordance with regulations of the Canadian Council on Animal Care. Adult male Sprague Dawley rats (>40 days old) were anesthetized with intraperitoneal injection of sodium pentobarbital (30 mg/kg) and perfused intracardially with ice-cold oxygenated (95% O_2 and 5% CO_2) sucrose-substituted artificial cerebrospinal fluid (ACSF) containing (in mM) 252 sucrose, 2.5 KCl, 2 $CaCl_2$, 2 $MgCl_2$, 10 glucose, 26 $NaHCO_3$, 1.25 NaH_2PO_4, and 5 kynurenic acid. The brain was rapidly removed and sectioned coronally to produce 400 μm-thick slices. Slices were kept in normal oxygenated ACSF (126 mM NaCl instead of sucrose and without kynurenic acid) at room temperature until recording.

Slices were transferred to a recording chamber constantly perfused with oxygenated (95% O_2 and 5% CO_2) ACSF heated to between 30 and 31°C. The slice was viewed with a modified Zeiss Axioplan2 microscope. Pyramidal neurons in the CA1 region of hippocampus were targeted for patching and were recorded from in the whole cell configuration with >80% series resistance compensation using an Axopatch 200B amplifier (Axon Instruments; Foster City, CA). Recording pipettes with Sylgard-coated shanks were filled with an intracellular solution composed of (in mM) 135 $KMeSO_4$, 5 KCl, 10 HEPES, and 2 $MgCl_2$, 4 ATP (Sigma), 0.4 GTP (Sigma) as well as 0.1% Lucifer Yellow; pH was adjusted to 7.2 with KOH. Intracellular Ca^{2+}

was left deliberately unbuffered in order not to disturb currents mediating adaptation (Marrion et al., 1991; Schwindt et al., 1992; Staley et al., 1992; Zhang et al., 1994). Following recording, pyramidal morphology was confirmed using epifluorescence to visualize intracellular labeling with Lucifer Yellow.

Reported values of membrane potential (V) were corrected for liquid junction potential. Neurons were judged healthy on the basis of three criteria: resting V < -50 mV, spikes overshooting 0 mV, and R_{in} >100 MΩ. Variation in resting V was eliminated by adjusting V in all cells to -70 mV through tonic injection of current. Access resistance was monitored during recording and testing was discontinued if it rose unrecoverably above 15 MΩ. All experiments were performed in 10 μM bicuculline methiodide (Research Biochemicals, Natick, MA), 10 μM 6-cyano-7-nitroquinoxaline-2,3-dione (CNQX), and 40 μM D-2-amino-5-phosphonovaleric acid (D-AP-5, Tocris Cookson, Bristol, UK) to block background synaptic activity. Neurons were excited by injecting 15 s-long current steps (I_{DC}) through the recording pipette.

Membrane conductance of the recorded neuron was manipulated through the dynamic clamp technique (Sharp et al., 1993) using a Digidata 1200A ADC/DAC board (Axon Instruments) and DYNCLAMP2 software (Pinto et al., 2001) running on a dedicated processor. Update rate was 10 kHz. Shunting was simulated as a constant conductance (g_{shunt}) with a reversal potential of -70 mV. The effect of different conductance levels was quantified in each neuron by measuring R_{in} based on a series of hyperpolarizing current pulses. The membrane time constant was determined (from the same responses used to calculate R_{in}) as the slowest time constant from exponential curve fits.

Traces were low-passed filtered at 4 kHz and stored on videotape using a digital data recorder (VR-10B, Instrutech Corp.; Port Washington, NY). Off-line, recordings were sampled at 10 kHz on a computer using Strathclyde Electrophysiology software (J. Dempster, Department of Physiology and Pharmacology, University of Strathclyde, Glasgow, UK) and analyzed using locally designed software (De Koninck).

Simulations

The phase plane model was based on the Morris-Lecar model (Morris and Lecar, 1981; Rinzel and Ermentrout, 1998), described by the following equations:

$$C\,dV/dt = I_{DC} + I_{noise} + I_{signal} - g_{Na}\cdot m_\infty(V)(V-E_{Na}) - g_K\cdot w(V-E_K) - g_{shunt}(V-E_{shunt}) - g_{adapt}\cdot z(V-E_K) \quad [1]$$

$$dw/dt = \phi\,[w_\infty(V) - w] \,/\, \tau_w(V) \quad [2]$$

$$dz/dt = \alpha\,\{1 \,/\, [1+\exp(-\beta-V)/\gamma] - z\} \quad [3]$$

$$m_\infty(V) = 0.5\,\{1+\tanh[(V-V_1)/V_2]\} \quad [4]$$

$$w_\infty(V) = 0.5\,\{1+\tanh[(V-V_3)/V_4]\} \quad [5]$$

$$\tau_w(V) = 1 \,/\, \cosh[(V-V_3)/(2\cdot V_4)]. \quad [6]$$

Equations were integrated numerically in XPPAUT (Ermentrout, 2002) using the Euler method with a time step of 0.1 ms. Parameters were found by systematically varying them in order to recreate critical response characteristics in the model neuron, most notably, the sensitivity of repetitive spiking to membrane conductance. They were as follows: $C = 2$ μF/cm^2, $g_{Na} = 20$ mS/cm^2, $E_{Na} = 50$ mV, $g_K = 20$ mS/cm^2, $E_K = -100$ mV, $E_{shunt} = -70$ mV, $\phi = 0.15$, $V_1 = -1.2$ mV, $V_2 = 23$ mV, $V_3 = -2$ mV, and $V_4 = 21$ mV. The above parameters give rise to type II excitability; the model was also tested with $V_3 = 10$ mV to confirm results in a model with type I excitability. To modulate membrane conductance, g_{shunt} was varied between 2 and 5.3 mS/cm^2. DC stimulus intensity was controlled by I_{DC} and was adjusted to compensate for the decreased excitability caused by shunting, thereby facilitating comparison of responses across conductance levels.

Two variations of adaptation were tested, both based on the formalism described by Ermentrout (1998) (see Equation 3). Parameters for the M current were $g_{adapt} = 2$ mS/cm^2, $\alpha = 0.005$, $\beta = -35$ mV, $\gamma = 5$ mV. Parameters for a calcium-activated potassium (AHP) current were $g_{adapt} = 15$ mS/cm^2, $\alpha = 0.005$, $\beta = 0$ mV, $\gamma = 5$ mV. The important difference is voltage at half-maximal activation (controlled by β) which when set to 0 mV, ensures that adaptation is induced only during spikes (for the AHP current), whereas when set to -35 mV, allows adaptation to be induced at subthreshold voltages (for the M current). g_{adapt} was adjusted so that steady-state

firing rate in response to constant stimulation in the low conductance state was equivalent for both types of adaptation.

Although voltage oscillations similar to those seen experimentally could be observed in the model neuron using the parameters described above, a small amount of noise was introduced in order to make these oscillations less regular and therefore more in accordance with electrophysiological data. I_{noise} is considered to represent intrinsic noise sources and was modeled as an Ornstein-Uhlenbeck process (Uhlenbeck and Ornstein, 1930),

$$dI_{noise}/dt = -I_{noise}/\tau_{noise} + \sigma_{noise}N(0,1) \quad [7]$$

where $N(0,1)$ is a number drawn from a Gaussian distribution with average 0 and unit variance, which is then adjusted according to size of the time step (Destexhe et al., 2001). Noise amplitude was controlled by a scaling factor, σ_{noise}; τ_{noise} = 5 ms and σ_{noise} = 0.5 $\mu A/cm^2$. I_{noise} was removed from the model neuron when investigating bifurcation patterns.

In one set of simulations investigating spike-time precision, a 20 ms-long current step was superimposed on the DC stimulus. Latency to spike from the onset of stimulation was measured, and the cumulative distribution of latencies was compared between conditions using the Kolmogorov-Smirnov test. Width of the latency distribution can be equated with the reciprocal of spike-time precision. In a separate set of simulations, the model neuron was stimulated with a dynamic input signal, I_{signal}, that was generated through an Ornstein-Uhlenbeck process. Unlike I_{noise} which varied with each trial, I_{signal} was recorded on one trial and replayed on all subsequent trials, such that the signal represents "frozen noise". τ_{signal} = 5 ms and σ_{signal} was varied. Spike-time precision was calculated using the correlation-based method described by Schreiber et al. (2003). Briefly, each spike train was convolved with a Gaussian filter (σ_{filter} = 0.5 ms) and were then correlated pairwise by taking the inner product followed by normalization. Each spike train was generated by a 5 s-long stimulus where the first 500 ms, during which adaptation develops, was excluded from analysis. Based on 10 trials in each condition, the final precision metric was based on measurements averaged across 45 pairwise correlations.

RESULTS

Experimental observations in CA1 pyramidal neurons

In the six CA1 pyramidal neurons upon which subsequent analysis is based, application of a 10 nS shunt by dynamic clamp reduced average R_{in} from 158.5 ± 9.4 MΩ to 69.7 ± 9.4 MΩ ($p < 0.001$, paired *t*-test). This equates to a 56% drop in R_{in}, which conservatively approximates conditions *in vivo* (Destexhe and Paré, 1999). The decrease in R_{in} was accompanied by a 56% reduction in the membrane time constant and caused a predictable reduction in excitability. For the cell illustrated in Figure 1A, ~160 pA greater stimulation was necessary to achieve the same initial firing rate (calculated from the first interspike interval) in the high conductance state compared to in the low conductance state (Fig. 1B). Despite compensating for decreased excitability by increasing stimulus intensity to elicit the same initial firing rate, the number of spikes in the initial burst was consistently fewer in the high conductance state compared to in the low conductance state (Fig. 1C) and spiking after the initial burst was abolished in the high conductance state, whereas slow repetitive spiking persisted in the low conductance state (Fig. 1D). These observations demonstrate that simply increasing stimulus intensity cannot fully compensate for the effects of shunting.

Since burst duration and steady-state firing rate are both modulated by adaptation, the above data suggested that shunting and adaptation interact to determine the spiking response. Moreover, this interaction must be nonlinear since even extremely strong stimulation can not cause the shunted neuron to fire repetitively (Fig. 1A), thereby disproving that effects of adaptation and shunting are simply additive. To isolate how shunting influences adaptation, the direct effects of shunting on excitability were removed by plotting burst duration and steady-state firing rate against initial firing rate (Fig. 1E and F, respectively) rather than against stimulus intensity (as in Fig. 1C and D). After accounting for variation in initial firing rate, the initial burst was significantly shorter in the high conductance state (Fig. 1E; $p < 0.001$, ANOVA) and steady-state firing rate was significantly lower in the high conductance state (Fig. 1F; $p < 0.001$, Kruskal-Wallis test).

Influence of shunting on adaptation can be reproduced in a phase plane model

To investigate the nonlinear interaction between shunting and adaptation, we developed a phase plane model that was able to reproduce the experimental data in Figure 1. For the model neuron reported in Figure 2, adaptation was mediated through an M current. Sample responses are shown in Figure 2A. As observed in real CA1 pyramidal neurons, shunting caused a rightward shift in the $f_{initial}$-I_{DC} curve (Fig. 2B), shortened the initial burst of spikes (Fig. 2C), and prevented steady-state firing (Fig. 2D) in the model neuron. Analysis of the model revealed that repetitive spiking was generated through a subcritical Hopf bifurcation in both the low and high conductance states (Fig. 2E) (see Rinzel and Ermentrout (1998) for review of bifurcations in the context of neuronal excitability). Shunting did not therefore cause a qualitative change in the mechanism through which spikes were generated, but the values of I_{DC} and V at which the bifurcation occurred (referred to as I_* and V_*, which correspond to rheobase and voltage threshold, respectively) did change. Since the change in I_* confers reduced excitability that can be overcome with increased stimulation, we investigated whether the change in V_* underlies the effects of shunting on adaptation.

The results above are from a model neuron exhibiting type II excitability. In order to demonstrate the generality of our findings before proceeding with more detailed analysis, we also tested a model neuron exhibiting type I excitability. Type I and II excitability are distinguishable on the basis of the *f-I* curve (continuous vs. discontinuous near 0 Hz, respectively, based on ability of the neuron to spike slowly in response to just-suprathreshold stimulation) (Hodgkin, 1948) and the type of bifurcation associated with generation of repetitive spiking (saddle-node vs. Hopf, respectively) (Rinzel and Ermentrout, 1998). Sample responses from a neuron model with type I excitability (Fig. 2F) demonstrate that the interaction between shunting and adaptation has the same consequences in type I and II neurons (other data not shown).

Phase plane and bifurcation analyses of the interaction between shunting and adaptation

Adaptation is a negative feedback process that reduces firing rate via an outward,

transmembrane current whose induction is dependent on voltage in the case of the M current (Storm, 1990) or on intracellular calcium in the case of the AHP current (Sah and Davies, 2000). In the latter case, a calcium current need not be explicitly modeled if the activation curve for the AHP current (relative to voltage) is adjusted so that activation occurs exclusively during the spike (i.e. the same conditions under which calcium influx through high voltage-activated calcium channels would occur and activate the AHP current). Adaptation mediated by the M current is considered first, followed by comparison of those results with adaptation mediated by an AHP current. The proportional activation of adaptation (between 0 and 1) is reported as z.

During stimulation in the low conductance state, z increased incrementally with each spike and decayed between spikes (Fig. 3A, left panel) whereas with stimulation causing the same initial firing rate in the high conductance state, z was able to increase without co-occurring spikes (Fig. 3A, right panel). This difference in how z changes is explained by phase plane analysis, and specifically by how the z- and V-nullclines intersect (Fig. 3B). The V-nullcline represents all points in phase space where V remains constant, whereas the z-nullcline represents all points where z remains constant. The latter corresponds to the activation curve for adaptation. Although the two nullclines intersect at three points, only the bottom left point is important for the system's dynamics since, prior to stimulation, z starts at 0 and increases slowly. The stability of that point depends on how the z- and V-nullclines intersect: if they intersect at $V < V_*$, the point is stable whereas it is unstable if they intersect at $V > V_*$ (V_* corresponds to V at the trough of the V-nullcline and stability is determined from the eigenvalues found by local stability analysis near the fixed point). It is therefore important that the vertical position of the V-nullcline, and therefore how that nullcline intercepts the z-nullcline, is controlled by the balance of stimulation and adaptation: excitatory stimulation shifts the V-nullcline upward while adaptation shifts it downward.

Focusing first on the low conductance state, Figure 3B (left panel) shows that stimulation causes the *initial* V-nullcline to intersect the z-nullcline at $z \approx 0.35$. However, as z increases towards this new value, I_{adapt} increases and shifts the *adapted* V-nullcline downward. The z- and

adapted V-nullclines intersect at *z* between 0.12 and 0.15 (yellow shading on Fig. 3B), which corresponds to $V > V_*$ (green shading), meaning the unstable fixed point moves within the red region (Fig. 3B, left panel). If I_{adapt} had been strong enough to cause stabilization, *V* would be forced below V_*; lack of stabilization means that *V* remains above V_*. So long as voltage remains above threshold, spiking will continue. The onset and offset of spiking as *V* changes relative to V_* occurs through a Hopf bifurcation. A decrease in I_{DC} or an increase in g_{adapt} can strengthen adaptation relative to stimulus intensity so that the same proportional activation of I_{adapt} (i.e. caused by the same increase in *z*) can shift the *adapted V*-nullcline far enough down to stabilize the intersection point and abolish repetitive spiking (see below).

On the other hand, in the high conductance state (Fig. 3B right panel), I_{adapt} is able to shift the *V*-nullcline down far enough that the *z*- and *adapted V*-nullclines intersect at $V < V_*$, meaning the intersection point has stabilized and repetitive spiking is prevented. Notably, this occurred despite g_{adapt} and I_{DC} being comparable to values that did not prevent repetitive spiking in the low conductance state (specifically, g_{adapt} was equal and I_{DC} was increased only enough to compensate for reduced excitability caused by the shunt). The crucial observation is that the *V*-nullcline is shifted rightward in the high conductance state (Fig. 3B), reflecting the increase in V_* noted in Figure 2E. This horizontal shift alters the position of the *V*-nullcline relative to the *z*-nullcline, with two consequences: the same upward shift in the *V*-nullcline causes a greater increase in *z* (i.e. greater activation of adaptation) and stabilization of the system at $V < V_*$ requires a smaller downward shift in the *V*-nullcline (i.e. smaller value of I_{adapt}). Maintenance of the stable state requires that I_{adapt} remain strong enough to counterbalance I_{DC} so that *V* remains below V_*, which necessarily requires maintained activation of adaptation at subthreshold potentials. Figure 3C illustrates that subthreshold depolarization is able to activate the M current (as evident from the increase in *z*), and that this activation is much greater in the high conductance state compared to the low conductance state.

Bifurcation diagrams in Fig. 3D summarize changes in *z* and the resulting spiking pattern over a broad range of stimulus intensities. In the low conductance state (top panel), the fixed

point defined by the *V*- and *z*-nullclines becomes unstable at I_{DC} = 38 μA/cm^2. Less intense stimulation will either fail to produce a bifurcation, in which case no spiking or a single spike generated independently of a bifurcation occurs (region *i*, see also Fig. 2E) or adaptation will be strong enough to reverse the bifurcation, in which case spiking does not persist after the initial burst (region *ii*). For I_{DC} > 38 μA/cm^2, the fixed point destabilizes, allowing repetitive spiking that is either irregular (region *iiia*) or regular (region *iiib*) depending on the stability of the limit cycle. In the high conductance state (bottom panel), there is no equivalent of region *iiia* and, instead, a region of bistability exists where the stable fixed point and stable limit cycle overlap in region *iiib*, but the system evolves to the latter because *z* approaches from below.

In contrast to the above findings for M current-mediated adaptation, adaptation mediated through the AHP current was unable to abolish repetitive spiking (Fig. 4A). This is explained by the requirements for activating the AHP current: little if any activation is achieved at subthreshold potentials (Fig. 4B and C). Because of the resulting phase plane geometry, adaptation restabilizes the system through a saddle-node bifurcation (Fig. 4B), rather than through a Hopf bifurcation as for the M current; these bifurcations refer specifically to changes in the *z*-*V* phase plane and not to changes in the *w*-*V* phase plane. In order to restabilize the system, I_{adapt} would need to shift the *V*-nullcline back so that it intercepts the *z*-nullcline at *z* = 0, but that would necessarily mean I_{adapt} is inactivated. Since activation of the AHP current can not be maintained at subthreshold potentials (Fig. 4C), adaptation mediated through the AHP current can not prevent repetitive spiking. Changes in *z* and the resultant spiking pattern over a broad range of I_{DC} are summarized in the bifurcation diagrams in Figure 4D. Note that region *ii* is absent for both the low and high conductance states.

Having explained transitions between subthreshold responses and responses with and without repetitive spiking after the initial burst, we asked how bifurcation patterns observed in the model cell compared quantitatively with bifurcation patterns observed experimentally. Without imposing a shunt through dynamic clamp, four of six CA1 pyramidal neurons switched from a subthreshold response to a response without repetitive spiking before switching to

repetitive spiking, in other words, progressing from region *i* to *ii* to *iii*, as stimulus intensity was increased (Fig. 5A, left panel). However, two of six neurons switched directly from region *i* to *iii*, suggesting region *ii* is narrow or absent in certain cases (see below). When a 10 nS shunt was applied to the neurons, region *iii* was consistently absent and region *ii* became much wider (Fig. 5A, right panel). The experimental bifurcation pattern in the high conductance state is consistent with the actions of an M current (compare against bottom panels of Fig. 3D and 4D); extrapolation to the low conductance state would therefore argue that region *ii* is sometimes narrow, rather than absent. These observations prompted a more specific question: can the model neuron reproduce the narrowness of region *ii* in the low conductance state, and its substantial widening by increases in membrane conductance?

For the original model neuron with M current-mediated adaptation, adaptation completely abolished repetitive firing over a fairly broad range of I_{DC} in both the low and high conductance states; region *ii* was 52 and 56% as wide as region *i* in Fig. 3C, respectively, which does not account for the experimentally observed widening of region *ii*. We tried doubling g_{adapt}, and although this increased the size of region *ii* to 150% and 146%, respectively (relative to region *i*), the increase was roughly equal for both conductance levels. We next tried increasing g_{shunt} in order to reproduce precisely the relative drop in R_{in} observed experimentally; under these new high conductance conditions, V_* was -33.5 mV but this change alone did not substantially alter the relative size of region *ii*. We then steepened the activation curve for adaptation by decreasing γ to 2 (see Equation 3) so that little adaptation was induced at V_* associated with the low conductance condition, thereby exaggerating adaptation's differential activation depending on V_*. Under these new conditions, the size of region *ii* relative to region *i* shrunk to only 2% in the low conductance state, but expanded to 107% in the high conductance state. Furthermore, combining an increase in g_{adapt} with a decrease in γ enlarged region *ii* so much so in the high conductance state, that repetitive spiking (region *iii*) could not occur at physiological stimulus intensities; in contrast, region *iii* dominated for the same parameters in the low conductance state (Fig. 5B). This demonstrates that region *ii* can be arbitrarily narrow for one conductance level,

and become dramatically wider as membrane conductance increases, affirmatively answering the question posed above: a nonlinear interaction between shunting and adaptation can quantitatively explain the experimentally observed effects of membrane conductance on repetitive spiking.

Shunting-induced increase in voltage threshold

The above data have demonstrated the importance of a shunting-induced increase in voltage threshold. The increase in voltage threshold was identified on the basis of the bifurcation diagrams in Figure 2E. Here we consider why, in more biophysical terms, membrane conductance influences voltage threshold, and whether an increase in membrane conductance does indeed increase voltage threshold in real pyramidal neurons.

Figure 6A shows the first two spikes in response to step depolarization of the model neuron in the low and high conductance states. Voltage threshold can be identified as an inflection point when voltage is plotted against time (top traces in Fig. 6A), and as a local peak when the net transmembrane current ($I_{membrane}$) is plotted against voltage (bottom traces in Fig. 6A). In the $I_{membrane}$-V plots, the first spike is distinct from the second and all subsequent spikes because the delayed rectifier potassium current becomes activated in the latter case and contributes to $I_{membrane}$, but the horizontal position of the peak (which defines V_*) does not change. Based on the voltage response preceding the first spike, comparing between the low and high conductance states reveals the effects of shunting on the neuron's input resistance (black lines in Fig. 6B). Because the neuron is not purely passive, the $I_{membrane}$-V curve bends downwards as the sodium current is activated. Voltage at the peak of the $I_{membrane}$-V curve corresponds to the voltage beyond which any subsequent depolarization will increase the magnitude of inward sodium current faster than it will increase the magnitude of the outward leak current. Because the leak current is larger in the high conductance state, greater activation of the sodium current is necessary to increase the inward current sufficiently to counterbalance the larger outward current (Fig. 6B). Greater activation requires greater depolarization; hence, an increase in membrane conductance results in an increase in voltage threshold.

To summarize, experimental data reveal that repetitive spiking in response to sustained input is sensitive to the neuron's total membrane conductance. Simulation data show that this can be explained by a shunting-induced increase in voltage threshold that enhances the subthreshold activation of the M current. For this explanation to apply to real neurons, a shunting-induced increase in voltage threshold should be evident in the experimental data. Indeed, a 10 nS shunt significantly increased voltage threshold by 2.3 ± 0.5 mV (mean ± sem, $p < 0.01$, paired *t*-test).

Impact on spike-time precision and sensitivity to stimulus fluctuations

Whether or not shunting allows adaptation to prohibit repetitive spiking driven by constant input (henceforth referred to as complete and incomplete adaptation, respectively) should have important consequences for neuronal encoding. Using the terminology of Gutkin et al. (2003), complete adaptation prevents the neuron from generating spikes as an oscillator, forcing it to generate spikes uniquely as a threshold element. By extension, "background" spikes generated by an oscillating neuron may advance, delay, or prevent spikes evoked by a dynamic signal, meaning the timing of evoked spikes should be less precise if background spikes driven by DC input are not prevented by adaptation. Thus, timing of spikes evoked by a brief stimulus should be more precise in the high conductance state, where M current-mediated adaptation effectively prohibits repetitive spiking, compared to in the low conductance state, where adaptation fails to prohibit such spiking.

To test this prediction, we compared spike-time precision in response to a 20 ms-long step depolarization superimposed on a DC offset. The stimulus amplitude was 10% that of the DC offset. Figure 7A shows spike times for different combinations of shunting and adaptation. Evoked spikes showed the least jitter in the model neuron with M current-mediated adaptation in the high conductance state (bottom, left panel), whereas all other conditions showed examples of background spikes causing variable delays in the evoked spikes. That effect is evident in the rightward skew in the cumulative probability distributions of spike latency (Fig. 7B), whereas the distribution is clearly symmetrical in the case of M current-mediated adaptation in the high

conductance state. With the M current (Fig. 7B, left panel), shunting caused a significant narrowing of the spike latency distribution ($p < 0.05$, Kolmogorov-Smirnov test) without having any effect on the median latency, which was 4.1 and 4.2 ms for the low and high conductance states, respectively. With the AHP current (Fig. 7B, right panel), shunting significantly reduced the median latency from 5.4 to 2.3 ms ($p < 0.001$, Mann-Whitney test) which is attributable to the reduction of the membrane time constant by shunting, but after equalizing median latency, shunting did not significantly alter the spike latency distribution (inset in Fig. 7B). Comparing between the M and AHP currents, spike latency distributions were not significantly different for either conductance level after equalizing median latency (Fig. 7C, center panels). This was unexpected for the high conductance level since the M current was expected to be associated with a narrower distribution than the AHP current, based on the former's capacity to prevent background spikes and thereby improve spike-time precision. This result is readily explained by compression of the leftward skew by reduction of median latency for the AHP current (i.e. the distribution is shifted leftward but, since latency can not become negative, the distribution's left tail is compressed) such that the distributions become comparably narrow for the M and AHP currents despite the persistent rightward skew with the AHP current. Symmetrical narrowing associated with the M current is not attributable to this same mechanism, as median latency is unchanged by shunting. Indeed, if distributions are normalized by dividing each latency measurement by the median latency, the distributions for M and AHP current-mediated adaptation become significantly different in the high conductance state ($p < 0.01$, Kolmogorov-Smirnov test) (Fig. 7C, bottom right panel) but not in the low conductance state (Fig. 7C, top right panel).

These data therefore suggest that, regardless of the current mediating adaptation, strong stimulation can elicit precisely timed spikes, particularly if the membrane time constant is short, whereas weak stimulation elicits poorly timed spikes. For instance, in a model neuron with high membrane conductance and AHP current-mediated adaptation, reducing stimulus amplitude from 10% to only 3% of the DC offset caused the median latency to increase significantly from 2.3 to 4.7 ms ($p < 0.001$, Mann-Whitney test) (Fig. 7D, left panel). The increase in median latency was

associated with significant widening of the latency distribution ($p < 0.01$, Kolmogorov-Smirnov test) (Fig. 7D, center panel) which was abolished through normalization (i.e. dividing distribution by median latency) (Fig. 7D, right panel). Weaker stimuli clearly elicit less precisely timed spikes, which is not at all surprising (e.g. Mainen and Sejnowski, 1995). What is novel, however, is that reduction of stimulus intensity from 10% to 8% caused the model neuron with high membrane conductance and M current-mediated adaptation to fire an evoked spike in only 4% of trials. In other words, that neuron responded only to strong stimuli, but always did so with precisely timed spikes, whereas the neuron with AHP current-mediated adaptation was less selective in terms of stimulus intensity and consequently showed degraded spike-time precision as stimulus intensity was reduced.

These findings were investigated further using a different stimulus paradigm that involved a continuous dynamic signal instead of a discrete pulse. Figure 8A shows responses to this stimulus for different combinations of adaptation and shunting. As expected, spike-time precision (see Methods) increased as the amplitude of the signal, σ_{signal}, was increased (Fig. 8B). Values of σ_{signal} were chosen to allow comparison between equivalent σ_{signal} and between equivalent voltage fluctuations (since the magnitude of voltage fluctuations decreases with shunting) in the low and high conductance state. Although precision was consistently lower with AHP current-mediated adaptation compared with M current-mediated adaptation, this difference did not increase with shunting, as would have been expected from the data in Figure 7. This is explained by the fact that with a continuous signal, all spikes were evoked by stimulus fluctuations, preempting any background spikes that could have arisen (at a lower rate) from the DC input alone; thus, prevention of background spikes by an interaction between shunting and adaptation is inconsequential under these stimulus conditions. At the same time however, the interaction between shunting and adaptation is crucial for controlling sensitivity to stimulus fluctuations (Fig. 8C and D). In the high conductance state, the neuron with M current-mediated adaptation spiked only in response to $\sigma_{signal} > 3$ $\mu A/cm^2$, whereas smaller signals continued to elicit spikes with M current-mediated adaptation in the low conductance state or with AHP current-

mediated adaptation in either conductance state. The selectivity for strong stimuli results from tonic hyperpolarization produced by activation of the M current at perithreshold potentials (Fig. 8E), which acts to maintain a gap between average depolarization and voltage threshold that only large voltage fluctuations, driven by large stimulus fluctuations, can cross to elicit spikes. Membrane conductance is able to modulate this selectivity only when combined with the M current because, by adjusting voltage threshold, it can modulate activation of the M current at subthreshold voltages. By maintaining selectivity to strong stimuli, the combination of shunting and M current-mediated adaptation allows spike-time precision to remain high at low firing rates, whereas it would otherwise drop off precipitously (Fig. 8F).

Comparison of M and AHP current-mediated adaptation reveals crucial differences in how each current modulates spike generation (Fig. 8G). The AHP conductance (red/pink lines) increases upon spike generation and slowly decreases during the interspike interval, eventually allowing another spike to occur even in the absence of stimulation (excepting the DC offset). In other words, the neuron continues to act as an oscillator, but it becomes slower so that stimulus fluctuations have an opportunity to evoke spikes before background spikes occur. In contrast, the M conductance (blue/green lines) remains relatively constant throughout the interspike interval, especially in the high conductance state. As already explained, the magnitude of the M conductance changes significantly depending on the degree of shunting, which is evident in Fig. 8G by the vertical separation of the blue and green traces. Tonic hyperpolarization made possible by activation of the M current at subthreshold potentials not only prevents background spiking by converting the neuron from an oscillator to a threshold element but, further, limits spike generation to strong stimulus fluctuations which in turn helps ensure high spike-time precision; this control is relatively unaffected by latency from the last spike since the M conductance does not change much during the interspike interval. Although not discussed at length here, stimulus fluctuations must not only be large, but must also be reasonably fast in order to drive spike generation before (without) activating the M current. The shift from responding to constant input with repetitive spiking, to responding selectively to large, rapid

stimulus fluctuations with precisely timed spikes is, in every way, consistent with a conversion from integration to coincidence detection.

DISCUSSION

Experimental observations in hippocampal pyramidal neurons revealed that membrane conductance has a pronounced effect on the outcome of adaptation: adaptation was able to abolish repetitive spiking only when combined with increased membrane conductance. In order to explain how shunting and adaptation interact to control repetitive spiking, we developed a simplified phase plane model that reproduced the observed phenomenon. Effects of membrane conductance on the outcome of adaptation were explained by modulation of voltage threshold: adaptation sufficient to stabilize the system at subthreshold potentials is more likely to be induced when voltage threshold is increased by shunting. A shunting-induced increase in voltage threshold was observed experimentally, confirming that the proposed mechanism is applicable to real neurons. The increase in voltage threshold enhances subthreshold activation of the M current, but has no effect on the AHP current, explaining why only the former is able to abolish repetitive spiking. The nonlinear interaction between shunting and M current-mediated adaptation has important implications for encoding: brief stimuli evoke more precisely timed spikes when adaptation prevents background spikes elicited by DC input and, beyond that, good spike-time precision is ensured by allowing only large, rapid stimulus fluctuations to successfully evoke spikes. By modulating activation of the M current at subthreshold potentials, shunting can effectively control whether CA1 pyramidal neurons operate as integrators or as coincidence detectors.

As outlined in the Introduction, background synaptic activity such as occurs *in vivo* can cause a dramatic increase in total membrane conductance compared to values typically observed in slice experiments. It is therefore important to determine precisely what effects shunting has on the computational properties of neurons in order to understand how neurons operate *in vivo*. Increase in membrane conductance has been postulated to encourage operation of neurons as

coincidence detectors, rather than as integrators, thereby improving temporal resolution with which neurons respond to inputs (Destexhe et al., 2003; Shu et al., 2003; Rudolph and Destexhe, 2003). The results reported in this study are fully consistent with that view, but additionally reveal a novel and powerful mechanism by which this occurs. When the neuron spikes repetitively in response to sustained DC input, it is acting as an integrator; conversely, when adaptation prevents repetitive spiking, it prevents the neuron from acting as an integrator. The fact that adaptation's capacity to prevent repetitive spiking depends on membrane conductance means that membrane conductance can effectively control the neuron's operational mode. In the high conductance state, a broad range of DC stimulus intensities can depolarize the neuron to just-subthreshold potentials; this is achieved because the activation of adaptation is proportional to stimulus intensity. By resting just below threshold, the neuron is ideally positioned to respond to fluctuating inputs that are fast enough to elicit spikes before the negative feedback imposed by adaptation takes effect. In fact, subthreshold activation of the M current can control how closely average depolarization approaches threshold, thereby setting a lower bound on the amplitude of voltage fluctuations that are able to elicit spikes. In other words, the same mechanism that prevents repetitive spiking in response to constant input goes one step further in ensuring responsiveness to only stimulus fluctuations greater than a certain amplitude. The interaction between shunting and adaptation therefore prevents the neuron from acting as an integrator, or oscillator, and instead causes it to act as an ideal coincidence detector, or threshold element (Gutkin et al., 2003). Adaptation can be similarly conceptualized as implementing a high pass filter (Benda et al., 2005); our results suggest this is even more true when adaptation is combined with high membrane conductance.

Of course a neuron that spikes repetitively to DC stimulation may also respond to superimposed input. However, in that case, "background" spikes may alter the timing of spikes evoked by the signal of interest. Such a neuron could be said to operate as a perturbed oscillator (Gutkin et al., 2003), and is expected to exhibit poorer spike-time precision than a threshold element, which is exactly what we observed (Fig. 7). But whereas background spikes altered the

timing of spikes evoked by discrete inputs, spikes evoked by continuous, dynamic signals appeared to preempt background spikes (Fig. 8), which would seemingly nullify any benefits of prohibiting background spikes. In effect, a perturbed oscillator that oscillates slowly may produce evoked spikes with precision comparable to spikes produced by a true threshold element if stimulus fluctuations are large. However, spike-time precision decreases as the amplitude of stimulus fluctuations decreases, but whereas oscillators cannot help but respond to small fluctuations, threshold elements can control their sensitivity and spike only in response to large fluctuations that produce precisely timed spikes. This sensitivity-control is achieved by maintaining a gap between average membrane potential and voltage threshold that only sufficiently large fluctuations are able to cross. Thus, the observation that subthreshold activation of the M current not only prevents the neuron from responding to constant input, but also restricts it from responding to dynamic input smaller than a certain amplitude, explains why a neuron operating in a high conductance state with M current-mediated adaptation can maintain good spike-time precision even at low firing rates; in contrast, neurons with AHP current-mediated adaptation and/or neurons operating in a low conductance state can not maintain good precision at low firing rates.

CA1 pyramidal neurons are known to express multiple outward currents that mediate adaptation, including the voltage-dependent M current and the calcium-activated AHP current (Madison and Nicoll, 1984; Storm, 1990; Sah and Davies, 2000). Gu et al. (2005) have recently argued that the former is exclusively responsible for adaptation in CA1 pyramidal neurons. The results of this study highlight the importance of the M current, but do not exclude the potential contribution of other currents to adaptation. However, although one may be tempted to disregard the differences between adaptation mediated through one or the other current, and to treat the negative feedback process in a more generic manner, results presented here indicate that the computational consequences of each type of adaptation may be quite distinct. Both currents reduce firing rate, but there is a fundamental difference: the M current can abolish repetitive spiking whereas the AHP current cannot. Previous modeling work appears consistent with this

conclusion (Yamada et al., 1998). Extremely slow calcium kinetics may give the impression that adaptation mediated by an AHP current can abolish repetitive spiking (e.g. Pineda et al., 1999), and in pragmatic terms this may be true, but our dynamical systems analysis suggests that although the system may evolve slowly, it remains unstable and should therefore eventually spike. The differential capacity to control repetitive spiking, as well as the differential capacity to control sensitivity to stimulus fluctuations (see above), stem from differences between the activation curves for the two currents: whereas the M current has a fairly broad activation curve and can be activated at subthreshold potentials (Adams et al., 1982; Halliwell and Adams, 1982; Gutfreund et al., 1995; Wang and McKinnon, 1995; Wang et al., 1998), the AHP current is activated by calcium arriving via high-voltage activated calcium channels or by calcium released from intracellular stores, where both processes typically rely on spike generation (Davies et al., 1996; Pineda et al., 1998; Pineda et al., 1999). The capacity for activation at subthreshold potentials, and the modulability of that activation by shunting, allows the M current to influence spike generation in ways that are quite distinct from the AHP current.

On their own, both adaptation and shunting shape neuronal coding properties. To the best of our knowledge, this is the first demonstration that shunting can qualitatively alter the outcome of adaptation. Given that the membrane conductance of pyramidal neurons is significantly increased by synaptic input received *in vivo*, the nonlinear interaction between shunting and adaptation is important for understanding how neurons process inputs under physiological conditions. The fact that adaptation is itself subject to extensive modulation by various neurotransmitters (Madison and Nicoll, 1986; Nicoll, 1988; McCormick and Williamson, 1989; Barkai and Hasselmo, 1994; Pedarzani and Storm, 1995; Tang et al., 1997) adds to the complexity of the problem, and leads to the inevitable conclusion that neuronal coding properties are highly regulated. Understanding how neurons encode information will not only require that we identify the biophysical determinants of encoding, but will also require that we understand the interactions between those determinants. This is especially true if those interactions are nonlinear, as is the case for membrane conductance and adaptation.

REFERENCES

1. Adams PR, Brown DA, Constanti A (1982) M-currents and other potassium currents in bullfrog sympathetic neurones. J Physiol 330: 537-572.

2. Alger BE, Dhanjal SS, Dingledine R, Garthwaite J, Henderson G, King GL, Lipton P, North A, Schwartzkroin PA, Sears TA, Segal M, Whittingham TS, Williams J (1984) Brain slice methods. In: Brain Slices (Dingledine R, ed), pp 381-437. New York: Plenum Press.

3. Barkai E, Hasselmo ME (1994) Modulation of the input/output function of rat piriform cortex pyramidal cells. J Neurophysiol 72: 644-658.

4. Benda J, Longtin A, Maler L (2005) Spike-frequency adaptation separates transient communication signals from background oscillations. J Neurosci 25: 2312-2321.

5. Bernander Ö, Douglas RJ, Martin KA, Koch C (1991) Synaptic background activity influences spatiotemporal integration in single pyramidal cells. Proc Natl Acad Sci USA 88: 11569-11573.

6. Davies PJ, Ireland DR, McLachlan EM (1996) Sources of Ca^{2+} for different Ca^{2+}-activated K^{+} conductances in neurones of the rat superior cervical ganglion. J Physiol 495: 353-366.

7. Destexhe A, Paré D (1999) Impact of network activity on the integrative properties of neocortical pyramidal neurons in vivo. J Neurophysiol 81: 1531-1547.

8. Destexhe A, Rudolph M, Fellous JM, Sejnowski TJ (2001) Fluctuating synaptic conductances recreate in vivo-like activity in neocortical neurons. Neuroscience 107: 13-24.

9. Destexhe A, Rudolph M, Pare D (2003) The high-conductance state of neocortical neurons in vivo. Nat Rev Neurosci 4: 739-751.

10. Ermentrout B (1998) Linearization of F-I curves by adaptation. Neural Comput 10: 1721-1729.

11. Ermentrout B (2002) Simulating, Analyzing, and Animating Dynamical Systems: A Guide to XPPAUT for Researchers and Students. Philadelphia, PA: SIAM.

12. FitzHugh R (1961) Impulses and physiological states in theoretical models of nerve membrane. Biophys J 1: 445-466.

13. FitzHugh R (1969) Mathematical models of excitation and propagation in nerve. In: Biological Engineering (Schwan HP, ed), pp 1-85. Toronto: McGraw-Hill Book Company.

14. Gu N, Vervaeke K, Hu H, Storm JF (2005) Kv7/KCNQ/M and HCN/h, but not KCa2/SK channels, contribute to the somatic medium after-hyperpolarization and excitability control in CA1 hippocampal pyramidal cells. J Physiol 566: 689-715.

15. Gutfreund Y, Yarom Y, Segev I (1995) Subthreshold oscillations and resonant frequency in guinea-pig cortical neurons: physiology and modelling. J Physiol 483: 621-640.

16. Gutkin B, Ermentrout GB, Rudolph M (2003) Spike generating dynamics and the conditions for spike-time precision in cortical neurons. J Comput Neurosci 15: 91-103.

17. Halliwell JV, Adams PR (1982) Voltage-clamp analysis of muscarinic excitation in hippocampal neurons. Brain Res 250: 71-92.

18. Hodgkin AL (1948) The local changes associated with repetitive action in a non-medullated axon. J Physiol 165-181.

19. Izhikevich EM (2000) Neural excitability, spiking and bursting. Int J Bifurcat Chaos 10: 1171-1266.

20. Madison DV, Nicoll RA (1984) Control of the repetitive discharge of rat CA1 pyramidal neurones in vitro. J Physiol 354: 319-331.

21. Madison DV, Nicoll RA (1986) Actions of noradrenaline recorded intracellularly in rat hippocampal CA1 pyramidal neurones, in vitro. J Physiol 372: 221-244.

22. Mainen ZF, Sejnowski TJ (1995) Reliability of spike timing in neocortical neurons. Science 268: 1503-1506.

23. Marrion NV, Zucker RS, Marsh SJ, Adams PR (1991) Modulation of M-current by intracellular Ca^{2+}. Neuron 6: 533-545.

24. McCormick DA, Williamson A (1989) Convergence and divergence of neurotransmitter action in human cerebral cortex. Proc Natl Acad Sci USA 86: 8098-8102.

25. Morris C, Lecar H (1981) Voltage oscillations in the barnacle giant muscle fiber. Biophys J 35: 193-213.

26. Nicoll RA (1988) The coupling of neurotransmitter receptors to ion channels in the brain. Science 241: 545-551.

27. Paré D, Shink E, Gaudreau H, Destexhe A, Lang EJ (1998) Impact of spontaneous synaptic activity on the resting properties of cat neocortical pyramidal neurons in vivo. J Neurophysiol 79: 1450-1460.

28. Pedarzani P, Storm JF (1995) Dopamine modulates the slow Ca^{2+}-activated K^{+} current IAHP via cyclic AMP-dependent protein kinase in hippocampal neurons. J Neurophysiol 74: 2749-2753.

29. Pineda JC, Galarraga E, Foehring RC (1999) Different Ca^{2+} source for slow AHP in completely adapting and repetitive firing pyramidal neurons. Neuroreport 10: 1951-1956.

30. Pineda JC, Waters RS, Foehring RC (1998) Specificity in the interaction of HVA Ca^{2+} channel types with Ca^{2+}-dependent AHPs and firing behavior in neocortical pyramidal neurons. J Neurophysiol 79: 2522-2534.

31. Pinto RD, Elson RC, Szucs A, Rabinovich MI, Selverston AI, Abarbanel HD (2001) Extended dynamic clamp: controlling up to four neurons using a single desktop computer and interface. J Neurosci Methods 108: 39-48.

32. Rinzel J (1985) Excitation dynamics: insights from simplified membrane models. Fed Proc 44: 2944-2946.

33. Rinzel J, Ermentrout GB (1998) Analysis of neural excitability and oscillations. In: Methods in Neuronal Modeling: From Ions to Networks (Koch C, Segev I, eds), pp 251-291. Cambridge, MA: The MIT Press.

34. Rudolph M, Destexhe A (2003) Tuning neocortical pyramidal neurons between integrators and coincidence detectors. J Comput Neurosci 14: 239-251.

35. Sah P, Davies P (2000) Calcium-activated potassium currents in mammalian neurons. Clin Exp Pharmacol Physiol 27: 657-663.

36. Schreiber S, Fellous JM, Whitmer D, Tiesinga P, Sejnowski TJ (2003) A new correlation-based measure of spike timing reliability. Neurocomputing 52-54: 925-931.

37. Schwindt PC, Spain WJ, Crill WE (1992) Effects of intracellular calcium chelation on voltage-dependent and calcium-dependent currents in cat neocortical neurons. Neuroscience 47: 571-578.

38. Sharp AA, O'Neil MB, Abbott LF, Marder E (1993) The dynamic clamp: artificial conductances in biological neurons. Trends Neurosci 16: 389-394.

39. Shu Y, Hasenstaub A, Badoual M, Bal T, McCormick DA (2003) Barrages of synaptic activity control the gain and sensitivity of cortical neurons. J Neurosci 23: 10388-10401.

40. Staley KJ, Otis TS, Mody I (1992) Membrane properties of dentate gyrus granule cells: comparison of sharp microelectrode and whole-cell recordings. J Neurophysiol 67: 1346-1358.

41. Storm JF (1990) Potassium currents in hippocampal pyramidal cells. Prog Brain Res 83: 161-187.

42. Tang AC, Bartels AM, Sejnowski TJ (1997) Effects of cholinergic modulation on responses of neocortical neurons to fluctuating input. Cereb Cortex 7: 502-509.

43. Uhlenbeck GE, Ornstein LS (1930) On the theory of Brownian motion. Phys Rev 36: 823-841.

44. Wang HS, McKinnon D (1995) Potassium currents in rat prevertebral and paravertebral sympathetic neurones: control of firing properties. J Physiol 485: 319-335.

45. Wang HS, Pan Z, Shi W, Brown BS, Wymore RS, Cohen IS, Dixon JE, McKinnon D (1998) KCNQ2 and KCNQ3 potassium channel subunits: molecular correlates of the M-channel. Science 282: 1890-1893.

46. Yamada WM, Koch C, Adams PR (1998) Multiple channels and calcium dynamics. In: Methods in Neuronal Modeling: From Ions to Networks (Koch C, Segev I, eds), pp 137-170. Cambridge, MA: MIT Press.

47. Zhang L, Weiner JL, Valiante TA, Velumian AA, Watson PL, Jahromi SS, Schertzer S, Pennefather P, Carlen PL (1994) Whole-cell recording of the Ca^{2+}-dependent slow afterhyperpolarization in hippocampal neurones: effects of internally applied anions. Pflügers Arch 426: 247-253.

Figure 1. Shunting modulates the outcome of adaptation in hippocampal CA1 pyramidal neurons. **(A)** Sample responses to constant stimulation in a low and high conductance state (left and right traces, respectively). Horizontally aligned traces show responses with equivalent initial firing rate (based on reciprocal of first interspike interval). Stimulus intensity is indicated beside each trace. Despite increasing stimulus intensity to elicit the same initial firing rate in the low and high conductance states, the initial burst was shorter and the repetitive spiking was completely abolished in the high conductance state. **(B)** Based on the same cell illustrated in part *A*, shunting caused a rightward shift in the $f_{initial}$-I_{DC} curve. **(C)** Shunting also reduced the number of spikes in the initial burst. **(D)** Whereas slow, repetitive spiking could persist after adaptation in the low conductance state, repetitive spiking was absent after adaptation in the high conductance state. **(E)** Plotting initial firing rate against other response measures removes the direct effect of shunting on excitability and helps isolate how shunting influences the outcome of adaptation. For parts *E* and *F*, top graphs show data for cell illustrated in part *A* and bottom graphs show cumulative data ($n = 6$ neurons, with 4-5 measurements per neuron for each condition). Lines in bottom graphs show linear regressions (low conductance, black line; high conductance, gray line). After accounting for variation in $f_{initial}$, there were significantly fewer spikes within the initial burst in the high conductance state compared to the low conductance state ($p < 0.001$, ANOVA). **(F)** Steady-state firing rate was also significantly lower in the high conductance state compared to the low conductance state ($p < 0.001$, Kruskal-Wallis test).

Figure 2. A modified Morris-Lecar model can reproduce the influence of shunting on repetitive spiking. **(A)** Sample responses from the model neuron in the low and high conductance states (left and right traces, respectively). Horizontally aligned traces show responses with equivalent initial firing rate. Stimulus intensity is indicated beside each trace. As in real pyramidal neurons, the initial burst was shorter and repetitive spiking was absent in the high conductance state. Adaptation is mediated by an M current in the model tested here. **(B)** Shunting caused a rightward shift in the $f_{initial}$-I_{DC} curve. **(C)** It also reduced the number of spikes in the initial burst. **(D)**

Shunting also completely abolished steady-state spiking over the range of stimulus intensities tested here, although repetitive spiking could be achieved with much stronger stimulation (see Fig. 3D). **(E)** Bifurcation diagrams show that regardless of membrane conductance, repetitive spiking was generated through a subcritical Hopf bifurcation in the *w*-*V* plane. Stable fixed point, thick solid line; unstable fixed point, thick dashed line; stable limit cycle, thin solid line; unstable limit cycle, thin dashed line. In the low conductance state, the bifurcation occurred at $I_{DC} = I_* = 25.4$ μA/cm^2 and $V = V_* = -46.5$ mV. Those values increased to $I_* = 98.8$ μA/cm^2 and $V_* = -37.8$ mV in the high conductance state. Bifurcation diagrams were generated with adaptation removed from the model neuron. **(F)** Responses in the low and high conductance states are essentially the same in a model neuron with type I excitability (shown here) as in a model neuron with type II excitability (part *A*).

Figure 3. Effects of membrane conductance on repetitive spiking results from a nonlinear interaction between shunting and M current-mediated adaptation. **(A)** Sample responses in the model neuron (top traces) together with the proportional activation of adaptation, *z* (bottom traces) for low and high conductance states (left and right traces, with $I_{DC} = 40$ and 110 μA/cm^2, respectively). In the low conductance state, *z* decreases after the initial burst and only increases incrementally with each spike; by contrast, in the high conductance state, *z* continues to increase after the initial burst in the absence of co-occurring spikes (arrow). **(B)** The *z*-*V* phase plane explains the difference in adaptation pattern. Nullclines show area in phase space where a variable remains constant. *z*-nullcline is shown as dashed orange line. *V*-nullcline (solid lines) is shown before stimulation (gray, *no stim*), at the onset of stimulation before adaptation develops (pink, *initial*), and following adaptation (blue, *adapted*); excitatory I_{DC} shifts the *V*-nullcline upward whereas I_{adapt} (the outward current caused by adaptation) shifts it downward. An increase in membrane conductance shifts the *V*-nullcline to the right, which corresponds to an increase in V_* (purple line). This horizontal shift allows the same I_{DC} to cause a greater increase in *z* in the high conductance state compared to in the low conductance state (based on where the *initial V*-

nullcline and *z*-nullcline intersect), causing greater activation of I_{adapt}. It also allows the system to be stabilized at a subthreshold potential (based on where the *adapted V*-nullcline and *z*-nullcline intersect) as a result of less I_{adapt}. Black line shows *z*-*V* trajectory, which evolves towards the intersection point only if that point becomes stable (arrow in right panel); repetitive spiking continues if the intersection point remains unstable (within red region, where yellow and green shading overlap in left panel). An increase in V_* therefore potentiates the capacity of adaptation to stabilize the neuron at $V < V_*$ and thereby preclude repetitive firing. **(C)** Perithreshold stimulation in the low conductance state causes modest activation of the M current (evident by a small increase in *z*) whereas much greater activation is achieved in the high conductance state. Insets show the M current's activation curve relative to V_*; yellow shading highlights subthreshold activation. **(D)** Bifurcation diagrams show changes in *z* as I_{DC} is increased. Stable fixed point, solid black line; unstable fixed point, dashed black line; stable limit cycle, solid red line; unstable limit cycle, dashed red line. In the low conductance state (top), there are four regions: subthreshold (region *i*), no repetitive firing after adaptation (*ii*), repetitive firing that is irregular (*iiia*) or regular (*iiib*) after adaptation. In the high conductance state (bottom), region *iiia* is missing. The absolute size of region *ii* increased in the high conductance state, but its size relative to region *i* remained almost unchanged at 56% in the high conductance state compared to 52% in the low conductance state. The relative size of region *ii* can, however, increase dramatically depending on adaptation parameters (see Results and Fig. 5). Note that the transition from region *i* to *ii* is based on a bifurcation in the *w*-*V* plane (see Fig. 2E), which is why that transition is not associated with a change on the *z*-I_{DC} bifurcation diagrams in part *D*.

Figure 4. Adaptation mediated through an AHP current can not prohibit repetitive firing, regardless of membrane conductance. **(A)** Sample responses in the model neuron (top traces) and proportional activation of adaptation, *z* (bottom traces) for low and high conductance states (left and right traces, with I_{DC} = 40 and 110 μA/cm^2, respectively). Adaptation is mediated exclusively by an AHP current modeled as a voltage-dependent current activated only by

suprathreshold depolarization (see Methods). Regardless of membrane conductance, z decreases between spikes, allowing repetitive spiking to occur. **(B)** The rightward shift in the z-nullcline compared to the z-nullcline associated with the M current (compare with Fig. 3B) means that no adaptation is induced or maintained at subthreshold potentials. Because of this, I_{adapt} is unable to shift the V-nullcline down far enough that the system is restabilized at $V < V_*$. This is true regardless of membrane conductance. **(C)** Perithreshold stimulation is unable to activate the AHP current for either conductance level. Insets show the AHP current's activation curve relative to V_*; the shift in V_* is inconsequential for the activation of this current. **(D)** Bifurcation diagrams show changes in z as I_{DC} is increased. Stable fixed point, solid black line; unstable fixed point, dashed black line; stable limit cycle, solid red line; unstable limit cycle, dashed red line. Region *ii* (where adaptation prevents repetitive firing) is completely absent in both the low and high conductance states (top and bottom graphs, respectively).

Figure 5. The range of bifurcation patterns seen in real pyramidal neurons can be reproduced in the model neuron with M current-mediated adaptation. **(A)** Graphs show stimulus intensity at which CA1 pyramidal neurons changed from a subthreshold response to an initial burst followed by no repetitive firing (transition from region $i \rightarrow ii$, solid line) and from no repetitive firing to repetitive firing (transition from region $ii \rightarrow iii$, dashed line) plotted as cumulative probability across the six neurons tested. Labelled regions are defined by the median stimulus intensity at which a transition occurs. In the low conductance state (left panel), region *ii* was observed in four of six neurons, but its absence in two neurons suggests region *ii* can be extremely narrow (see Results); for purposes of plotting, an intermediate transition through region *ii* was assumed for transitions from region *i* to *iii*. In the high conductance state (right panel), region *ii* was consistently wide and region *iii* was never observed over the range of stimulus intensities tested. **(B)** In the model neuron, region *ii* can be arbitrarily narrow at one conductance level and dramatically widen as membrane conductance increases. For the bifurcation diagrams shown here, M current-mediated adaptation was adjusted such that $g_{adapt} = 4$ mS/cm^2 and $\gamma = 2$ mV.

Repetitive firing predominated in the low conductance state (left panel) as indicated by the breadth of region *iii* relative to region *ii*, whereas repetitive firing was completely abolished in the high conductance state (right panel) as indicated by the absence of region *iii* and widening of region *ii*. Stable fixed point, thick solid line; unstable fixed point, thick dashed line; stable limit cycle, thin solid line; unstable limit cycle, thin dashed line.

Figure 6. Explanation and experimental confirmation of a shunting-induced increase in voltage threshold. **(A)** The first two spikes elicited by step depolarization of the model neuron are shown for the low and high conductance states (left and right panels, respectively). Phases of the action potential are colored differently to help relate the voltage response plotted against time (top panels) with the relationship between $I_{membrane}$ and voltage (bottom panels). Inset in bottom left panel shows low power view; arrow represents direction of change in V and $I_{membrane}$ over time. $I_{membrane}$ represents the sum of all transmembrane currents and was calculated from the relationship $I_{membrane} = I_{DC} - C \cdot dV/dt$. Voltage threshold ($V_*$) is identifiable as an inflection point in the top panels and as a local peak in the bottom panels. **(B)** Overlying the initial responses for the low and high conductance states highlights the change in input resistance caused by shunting (compare black lines). Responses diverge from the black lines at depolarized voltages because of activation of the sodium current. The peak is defined by the voltage at which the inward (sodium) current increases more (because of voltage-dependent activation) than the outward (leak) current increases (because of increased driving force), meaning depolazation beyond V_* causes net $I_{membrane}$ to decrease. The sodium current must activate more in the high conductance state than in the low conductance state (compare lengths of vertical arrows) in order to counterbalance the leak current and reverse the direction of change in $I_{membrane}$ as voltage increases. Greater sodium current activation requires greater depolarization, explaining why an increase in membrane conductance causes an increase in V_*. **(C)** For experimental data, V_* was estimated from the voltage at which d^2V/dt^2 (which reflects the first derivative or rate of activation of $I_{membrane}$) exceeded a cutoff value defined as 5× the root-mean-square noise in the baseline d^2V/dt^2 trace.

Using responses to an arbitrarily chosen stimulus intensity of 40 pA greater than rheobase, we analyzed the second spike within each spike train since the second spike occurs before adaptation develops and its analysis is not confounded by initial membrane charging, as can occur with the first spike. Based on those measurements, introduction of a 10 nS shunt caused a significant increase in V_* ($p < 0.01$, paired t-test, $n = 6$) that averaged 2.3 ± 0.5 mV (mean ± sem).

Figure 7. Spike-time precision is significantly improved by the prevention of repetitive spiking achieved through the nonlinear interaction between shunting and M current-mediated adaptation. **(A)** Raster plots show spike times for different combinations of adaptation and membrane conductance. On each trial, the model neuron was stimulated with a 20 ms-long pulse (trace at bottom and marked by rectangle) superimposed on the DC current. Pulse magnitude was one tenth the DC current magnitude (4 and 11 $\mu A/cm^2$ for the low and high conductance states, respectively). For M current-mediated adaptation in the high conductance state (bottom left panel), evoked spikes showed little jitter. In all other cases, background spikes and perithreshold voltage fluctuations caused evoked spikes to be less precisely timed. **(B)** Cumulative probability distributions summarize variability in the latency of the evoked spike based on 50 trials in each condition. For M current-mediated adaptation (left panel), median latencies were 4.1 and 4.2 ms for the low and high conductance states, respectively, but distributions were significantly different ($p < 0.05$, Kolmogorov-Smirnov test). For AHP current-mediated adaptation (right panel), the median latency was 5.4 ms in the low conductance state but decreased to only 2.3 ms in the high conductance state ($p < 0.001$, Mann-Whitney test), but after equalizing the median to 0 (i.e. subtracting median latency from each measurement), the two distributions were not significantly different (inset). **(C)** After equalization (center panels), spike latency distributions were not significantly different between M and AHP current-mediated adaptation in the low or high conductance states (top and bottom panels, respectively). However, if the distributions were normalized by dividing the equalized latencies by the original median (right panels), the distributions were significantly different for the high conductance state ($p < 0.01$, Kolmogorov-

Smirnov test), but remained unaltered in the low conductance state. **(D)** In the high conductance state, if stimulus amplitude was decreased, the model neuron with M current-mediated adaptation stopped responding (data not shown), whereas the model neuron with AHP current-mediated adaptation kept responding but became less precise; for example, after reducing the stimulus from 10% to 3% of the DC offset, a spike was still elicited in 80% of trials, but the median latency increased significantly from 2.3 to 4.7 ms ($p < 0.001$, Mann-Whitney test) (left panel). The equalized latency distribution for 3% stimulation was significantly wider than for 10% stimulation ($p < 0.01$, Kolmogorov-Smirnov test) (center panel) but this difference was abolished by normalization (right panel). Effects of equalization and normalization demonstrate that compression of the leftward skew by reduction of median latency (as with AHP current-mediated adaptation) is not equivalent to the symmetrical narrowing of the distribution (as with the M current-mediated adaptation), and suggests a differential sensitivity to stimulus intensity may be important for understanding how adaptation and shunting control spike-time precision.

Figure 8. Activation of the M current at subthreshold potentials ensures high spike-time precision at low firing rates by modulating sensitivity to stimulus fluctuations. **(A)** Raster plots show spike times for different combinations of adaptation and conductance levels. In each trial, the model neuron was stimulated with the same dynamic stimulus (shown at bottom) generated by an Ornstein-Uhlenbeck process. Stimulus amplitude was scaled by σ_{signal}, which was 1.8 and 4 $\mu A/cm^2$ for the low and high conductance state, respectively, in order to elicit similarly sized voltage fluctuations. For this and all subsequent panels, DC current (I_{DC}) was 40 and 110 $\mu A/cm^2$ for the low and high conductance states, respectively. **(B)** Regardless of the current responsible for adaptation, spike-time precision calculated from 45 pairwise comparisons from 10 trials in each condition (see Methods) increased as σ_{signal} increased. Precision was consistently less with AHP current-mediated adaptation compared with M current-mediated adaptation for equivalent σ_{signal}, but these data did not reveal an interaction between shunting and adaptation inasmuch as the difference in precision between M current and AHP current-mediated adaptation

remained unchanged as conductance increased. Standard deviation of voltage fluctuations, SD_V. **(C)** Firing rate, on the other hand, was influenced differently by σ_{signal} and g_{shunt} depending on the current responsible for adaptation. With the AHP current, firing rate was relatively insensitive to changes in σ_{signal} or g_{shunt}, whereas with the M current, firing rate was dramatically reduced by increased membrane conductance despite high σ_{signal}. **(D)** To investigate this further, σ_{signal} was systematically varied while measuring firing rate. Shunting caused a dramatic reduction in sensitivity to stimulus fluctuations when adaptation was mediated through an M current, restricting spike generation to $\sigma_{signal} > 3$ $\mu A/cm^2$, but had virtually no effect with AHP current-mediated adaptation. This is because AHP current-mediated adaptation aims to maintain a constant firing rate, whereas M current-mediated adaptation aims to maintain a constant membrane potential (see below). Inset shows relationship between σ_{signal} and SD_V. **(E)** With g_{Na} and g_K set to 0 mS/cm^2 in order to prevent spike generation, comparison of average depolarization (top panel) reveals the outward rectification caused by activation the M current at perithreshold potentials. Unlike the M current's influence on average membrane potential, its slow kinetics restrict it from modulating the amplitude of fast voltage fluctuations (bottom panel). Data are for testing in high conductance state with $\sigma_{signal} = 4$ $\mu A/cm^2$. The resulting gap between average depolarization and voltage threshold ensures that neurons with M current-mediated adaptation generate spikes only in response to large stimulus fluctuations when operating in a high conductance state. **(F)** By responding exclusively to large stimulus fluctuations, the shunted neuron with M current-mediated adaptation can maintain high spike-time precision while firing at low rates, a feature that is not evident with other combinations of adaptation and conductance level. **(G)** Activation/deactivation of g_{adapt} (bottom traces) following spike (top traces) for stimulus parameters producing $f_{steady\text{-}state} \approx 18$ Hz. The AHP current modulates interspike interval by transiently activating and deactivating, thereby enforcing a certain regularity in the spike train. In contrast, activation of the M current is relatively constant throughout the interspike interval, especially in the high conductance state, producing tonic hyperpolarization that controls responsiveness to stimulus fluctuations. Despite the same firing rate, the M conductance is

substantially higher in the high conductance state compared to the low conductance state, whereas the AHP conductance is unaffected by shunting.

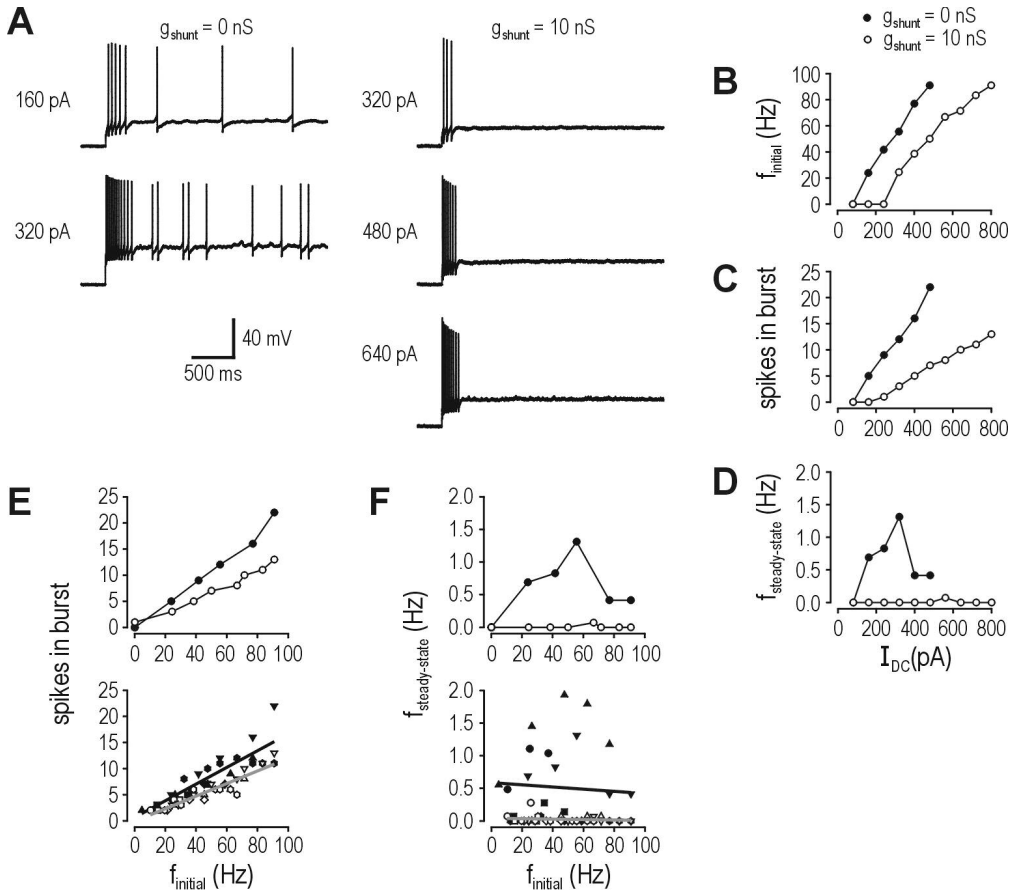

Figure 1. Shunting modulates the outcome of adaptation in hippocampal CA1 pyramidal neurons.

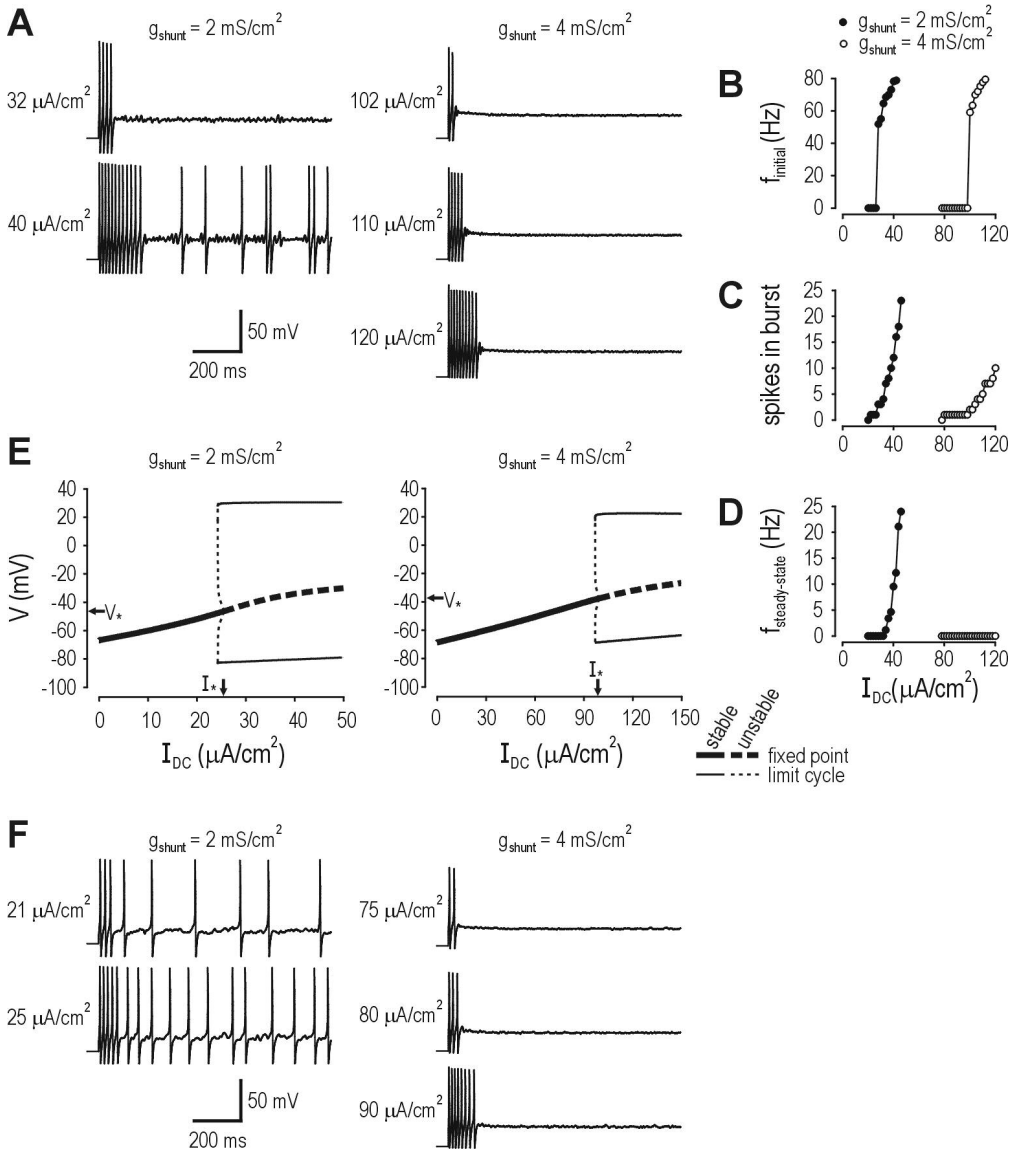

Figure 2. A modified Morris-Lecar model can reproduce the influence of shunting on repetitive spiking.

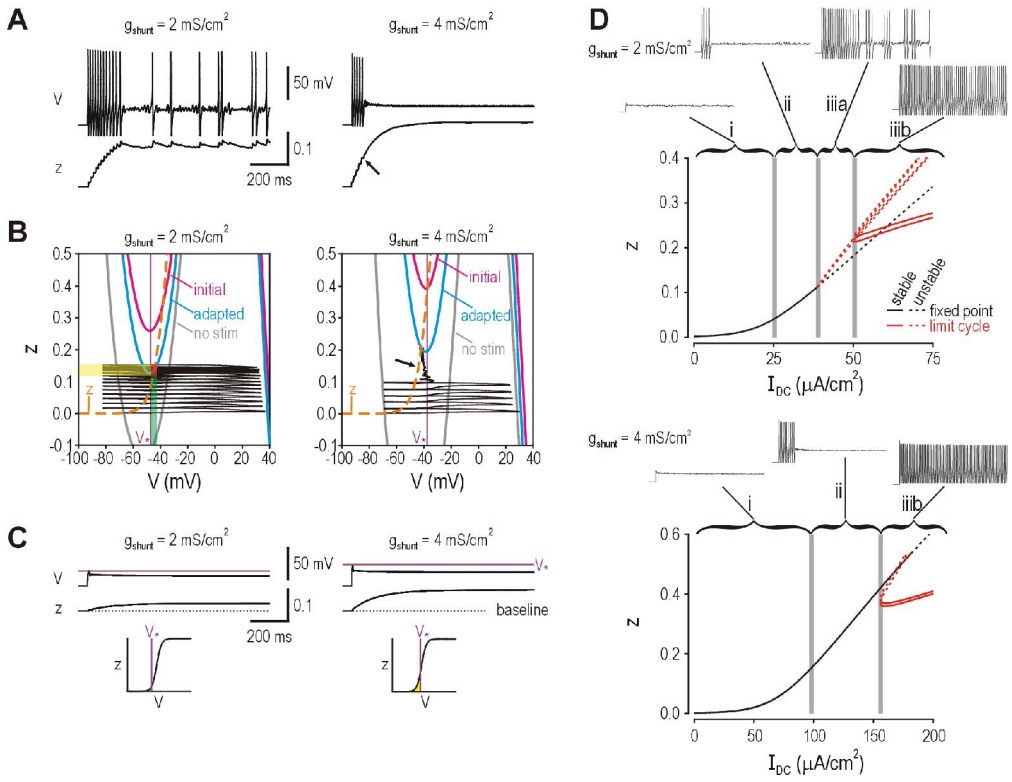

Figure 3. Effects of membrane conductance on repetitive spiking results from a nonlinear interaction between shunting and M current-mediated adaptation.

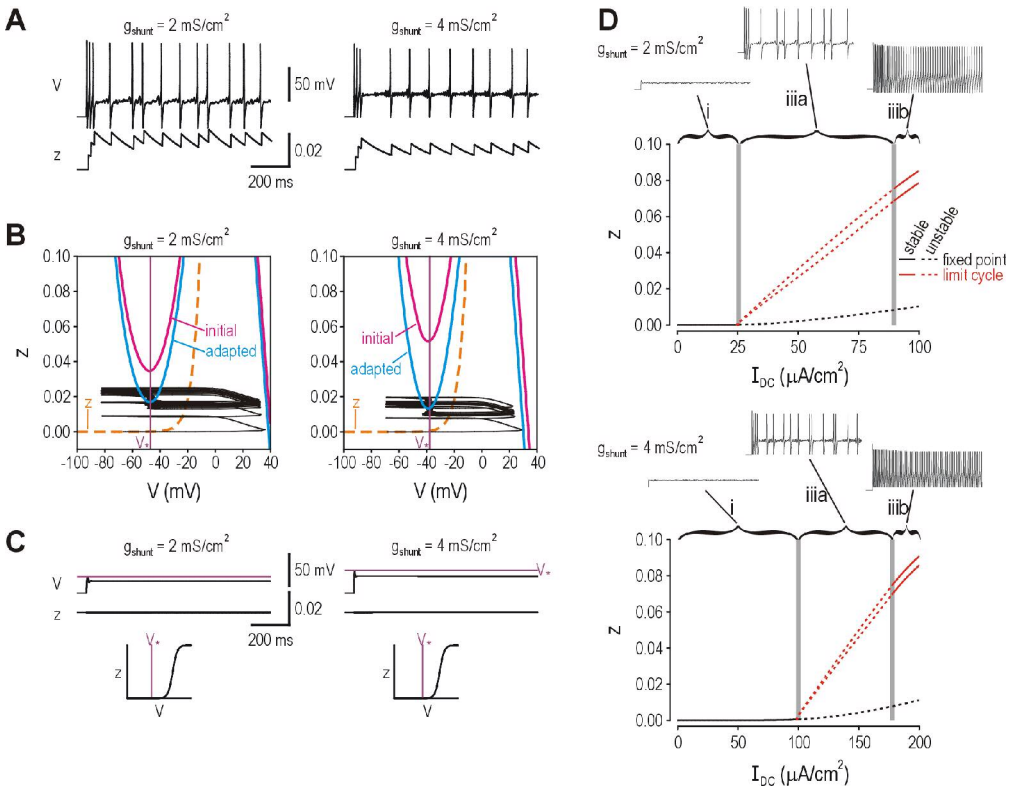

Figure 4. Adaptation mediated through an AHP current can not prohibit repetitive firing, regardless of membrane conductance.

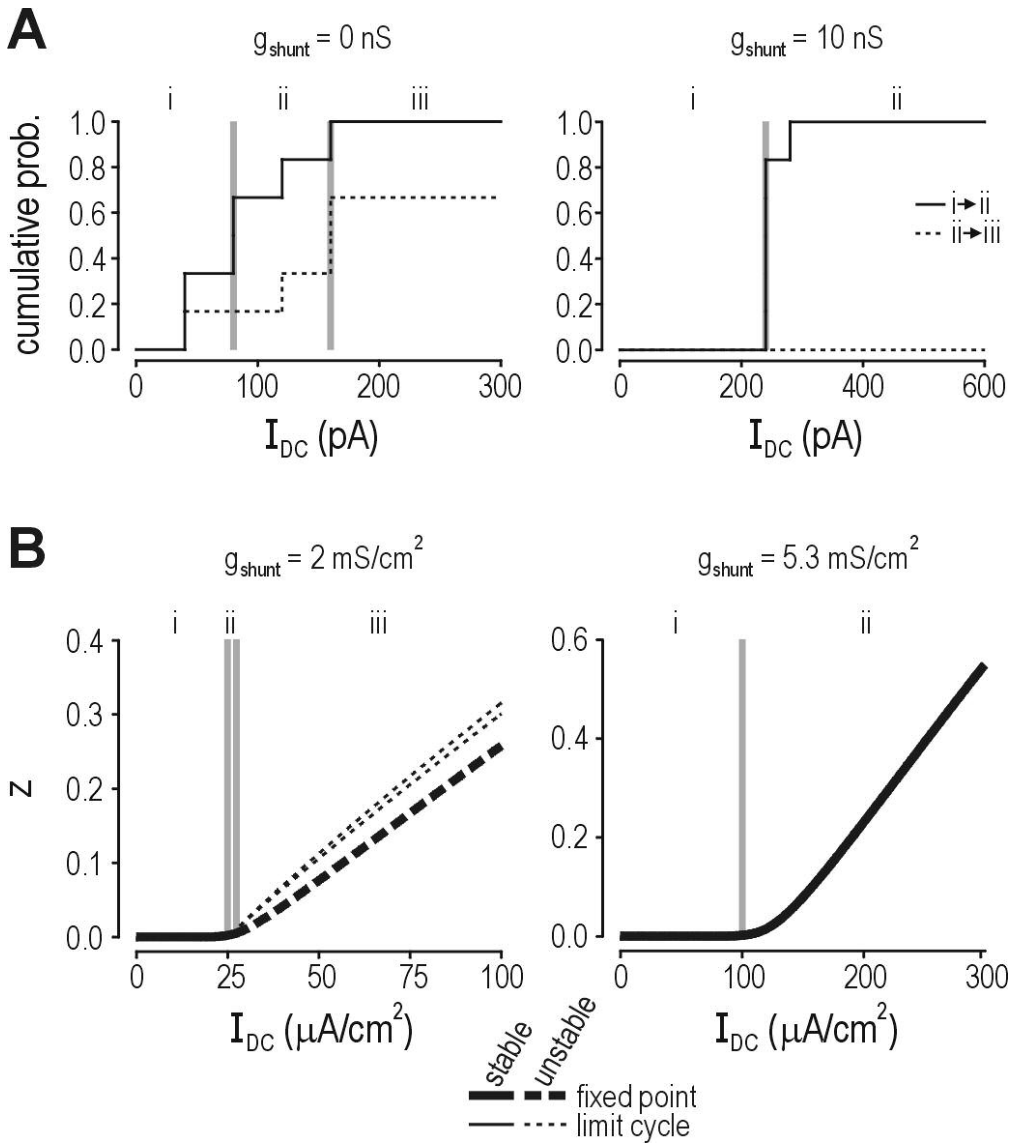

Figure 5. The range of bifurcation patterns seen in real pyramidal neurons can be reproduced in the model neuron with M current-mediated adaptation.

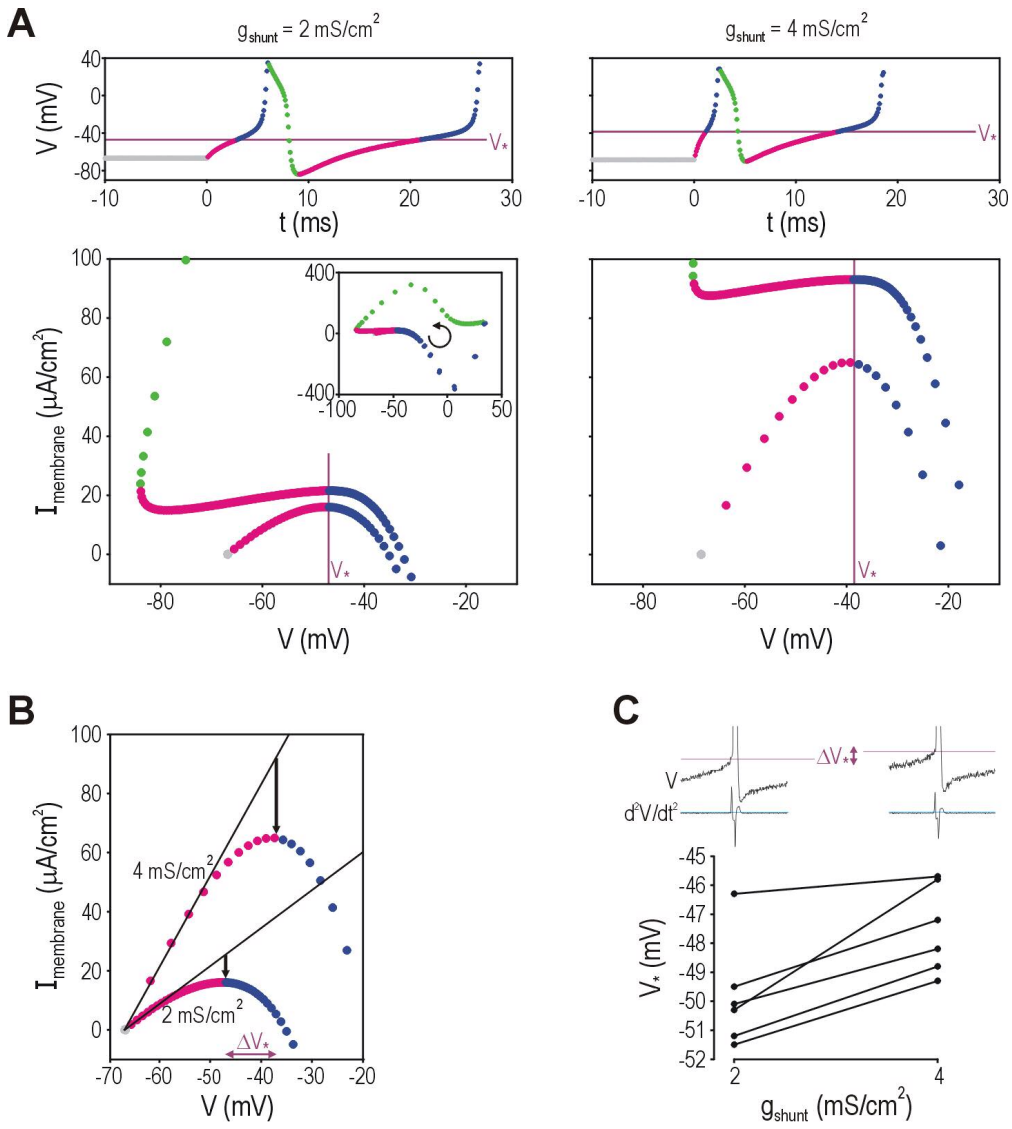

Figure 6. Explanation and experimental confirmation of a shunting-induced increase in voltage threshold.

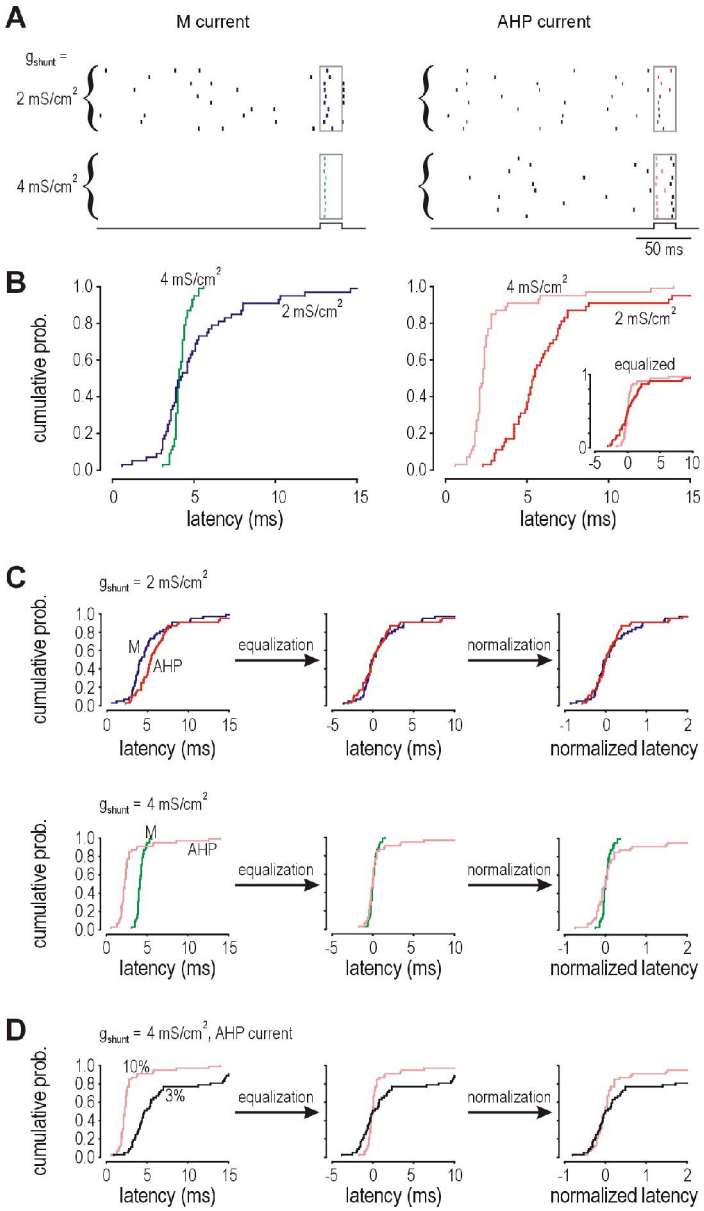

Figure 7. Spike-time precision is significantly improved by the prevention of repetitive spiking achieved through the nonlinear interaction between shunting and M current-mediated adaptation.

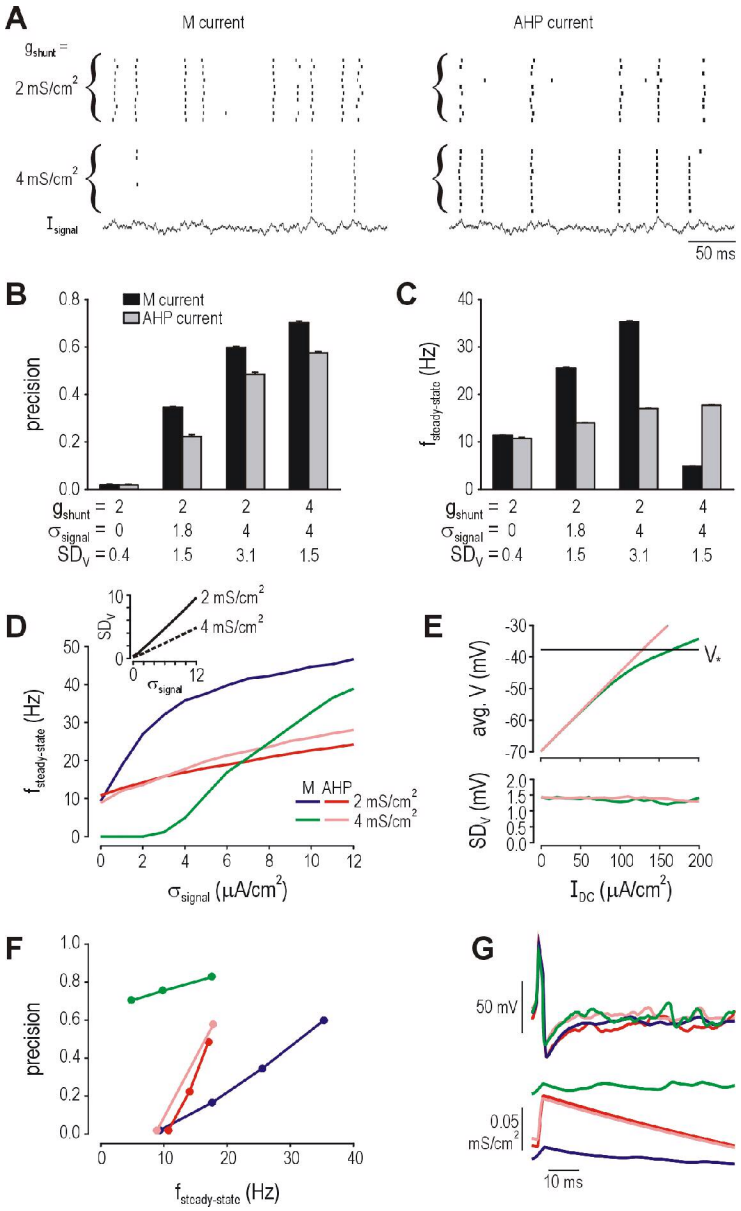

Figure 8. Activation of the M current at subthreshold potentials ensures high spike-time precision at low firing rates by modulating sensitivity to stimulus fluctuations.